

CFD thermal energy storage enhancement of PCM filling a cylindrical cavity equipped with submerged heating sources

T. Bouhal^{a,*}, Saïf ed-Din Fertahi^a, T. Kousksou^b, A. Jamil^a

^a Université Sidi Mohamed Ben Abdellah (U.S.M.B.A.), École Supérieure de Technologie de Fès, Route d'Imouzzer BP 2427, Morocco

^b Université de Pau et des Pays de l'Adour (UPPA/E2S), Laboratoire des Sciences pour l'Ingénieur Appliquées à la Mécanique et au Génie Electrique (SIAME) – Fédération IPRA, EA4581, 64000 Pau, France



ARTICLE INFO

Keywords:

PCM
Melting process
Thermal energy storage enhancement
Cylindrical cavity
CFD analysis

ABSTRACT

In this paper, two-dimensional CFD simulations were performed to simulate the melting process of a phase change material (PCM) filling a cylindrical cavity which includes heating sources. A CFD model based on the physical enthalpy-porosity formulation was used to simulate the phase change of the solid Gallium and to optimize the geometry of the heating sources according to the operating conditions in terms of the applied temperatures. The geometric effect of the heating sources, as well as the boundary conditions on the heat transfer characteristics are investigated in detail. In fact, the evolution of the temperature, liquid fraction and streamlines contours for the studied configurations, namely the cylindrical heating sources and the heating source with fins for two applied temperatures ($T_h = 40^\circ\text{C}$) and ($T_h = 45^\circ\text{C}$) were carried out. Temperature and liquid fraction measurement were assessed numerically for some specific points located inside the studied configurations for determining the redesign effect of the heating sources. Finally yet importantly, the heat transfer coefficient at the heating sources has been defined as indicator of performance to measure the contribution of the fins in the improvement of the melting time within the cylindrical cavity. It has been found that the cylindrical cavity where four fins are integrated at each heating source have enhanced the heat transfer in the PCM and improved its melting time from 18.35 min to 13.35 min while applying a hot temperature ($T_h = 40^\circ\text{C}$). Furthermore, the configuration with fins enhanced the heat transfer and improved the melting time of the PCM.

1. Introduction

Thermal energy storage (TES) improvement using phase change materials (PCMs) has become a highly topical issue of major importance in the scientific research community, because the released works with regard to this field have increased [1,2] during the last 20 years. It must be emphasized that research on the theory and application of phase change materials (PCM) in storage systems was undertaken extensively after 1970s [3]. In fact, the number of numerical and experimental studies has increased considerably. For instance, Diarce et al. [4] developed a two-dimensional CFD model for a new active type of ventilated facade integrating PCMs in their outer layer. They have shown that it is possible to consider a PCM as a solid material with a variable specific heat under the assumption of a negligible convective effects or thermal hysteresis phenomena. The expensive time of their numerical simulations was decreased using their developed melting and solidification model.

In the literature reports, Tay et al. [5] validated their CFD melting model against experimental results of a PCM encapsulated inside a

cylindrical tank which is intended for thermal energy storage applications. They concluded that the CFD developed model is predicting with accuracy the behavior of the storage system during the thermal storage and release energy phases. While Sattari et al. [6] simulated the melting process of PCMs within a spherical capsule. Furthermore, Liu et al. [7] have studied the integration of phase change materials into concrete through microencapsulation using cenospheres.

Kumarasamy et al. [8] developed new CFD numerical schemes to model the dominant heat transfer by conduction of PCMs, which are encapsulated. Moreover, investigating the heat transfer of a building brick that includes PCMs has been presented in [9]. Saffari et al. [10] released a review on passive cooling of buildings which are actually using PCMs. While Wang et al. [11] have conducted a study to enhance heat transfer using phase change composite material with copper, foam and paraffin. In addition to this, Kuznik et al. [12] have studied the impact of the enthalpy function on the simulation of a building with phase change material wall.

Park et al. [13] have performed a numerical model and simulation of a vehicular heat storage system with PCMs. Furthermore, Zhou et al.

* Corresponding author.

E-mail address: bouhal.tarik12@gmail.com (T. Bouhal).

Nomenclature		Ra	Rayleigh number
<i>Greek symbols</i>			
T_h	hot temperature (K)	ϕ_{int}	internal diameter (m)
T_c	cold temperature (K)	ϕ_{ext}	external diameter (m)
t	time (s)	ρ	density (kg/m^3)
\vec{u}	velocity vector (m/s)	$\overline{\tau}$	viscous stress tensor (Pa)
g	gravity (m/s^2)	β	thermal expansion coefficient (1/K)
T	temperature (K)	μ	viscosity (Pa s)
T_m	mean temperature (K)	α	liquid fraction
H	enthalpy (J)	λ	conductivity (W/K m)
h	sensible enthalpy (J)		
h_{ref}	reference enthalpy (J)		
C_p	specific heat capacity ($\text{J}/\text{K kg}$)		
T_s	solidus temperature (K)		
T_l	liquidus temperature (K)		
L_F	latent heat of melting (K)		
S	source term		
A_{mush}	mushy zone constant		
\vec{u}_p	solid velocity (m/s)		
<i>Abbreviations</i>			
PCM	phase change material		
CFD	computational fluid dynamics		
H.S	heat source		

[14] have conducted a dynamic measurement of the thermal conductivity of phase change materials in the liquid phase near the melting point. Besides, Browne et al. [15] have investigated the corrosive properties of phase change materials in contact with metals and plastic. The thermal performance of an integrated collector storage solar water heater (ICSSWH) with phase change materials (PCM) has also been investigated [16]. The modeling and analysis of phase change materials for efficient thermal management strategy has been carried out in [17].

Recently, Ma et al. [18] have conducted a review and outlook on the use of phase change materials in photovoltaic systems for thermal regulation and electrical efficiency improvement. Besides, Muhammad et al. [19] have performed the validation of a CFD melting and solidification model for phase change in vertical cylinders. Moreover, Sharma et al. [20] have presented a numerical study to enhance the solidification of phase change materials using trapezoidal cavity. In addition, Pielichowska et al. [21] have investigated the phase change materials for thermal energy storage. Temirel et al. [22] have studied the solidification of additive-enhanced phase change materials in spherical enclosures with convective cooling. Other interesting studies can be found in the literature treating the incorporation and heat transfer optimization of PCM modules. In fact, Cano et al. [23] have investigated experimentally the thermal storage system using phase change materials. Zhao et al. [24] have proposed a passive thermal management system for electronic device using low-melting-point alloy as phase change material. Furthermore, Kapsalis et al. [25] have

studied the solar thermal energy storage and heat pumps with phase change materials. Last but not least, Zhao et al. [26] have studied the heat transfer analysis of encapsulated phase change materials.

It should be noted that PCMs could be integrated inside stratified horizontal storage tanks [27], which include heat pipes [28] or vertical solar tanks [29] storage tanks to enhance their efficiency. Bouhal et al. [30] have already performed CFD parametric studies to optimize the energy efficiency of solar horizontal storage tanks and circulation pipes integrating evacuated tube collectors (ETC), by changing the number of the integrated heat pipes also their shape. It can be suggested as further studies to this thermal storage enhancement the integration of PCM within the tank, and to assess their effect on its overall efficiency such as the MIX number or the discharging yield. Further, PCMs can also be used to increase the efficiency of solar tanks linked to solar collectors for individual [31] or collective [32] applications of solar hot water production.

From our literature review and according to the best of the authors' knowledge, little attention has been paid to the heat transfer problem during the melting of the PCM heated from the outer surface of a closed cavity and from discrete sources with different shapes (internal heated cylinders with and without fins configurations) put at its inside. In this vision, this paper focuses on the melting process inside a cylindrical cavity, where a relatively higher temperature than the melting temperature of the PCM is applied. The effect of the internal heated source geometries, which are with and without fins on the kinetics of the

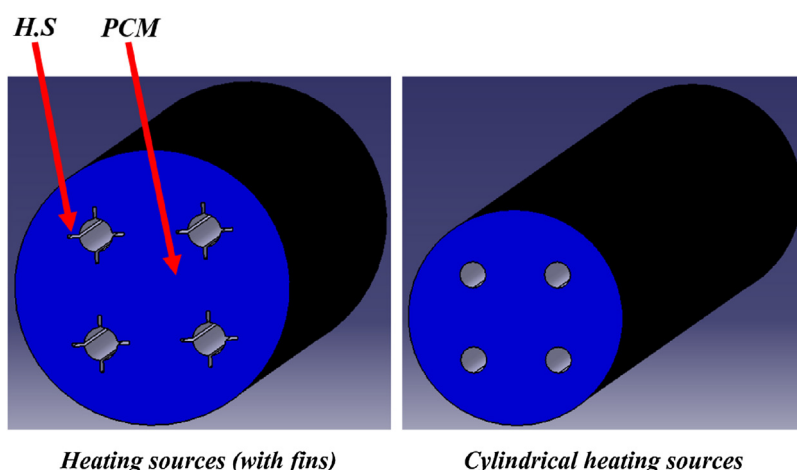


Fig. 1. Layout of the cylindrical cavity including heating sources with and without fins.

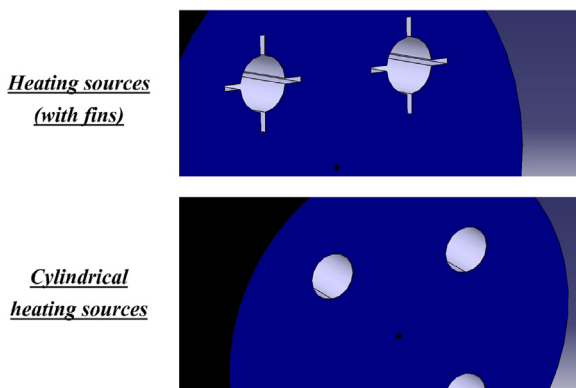


Fig. 2. Schematic of cylindrical heating sources and heating sources with fins.

Table 1
Physical properties of pure Gallium.

Density (liquid)	6093 kg m ⁻³
Reference density	6095 kg m ⁻³
Reference temperature	29.78 °C
Thermal expansion coefficient of liquid	1.2 × 10 ⁻⁴ K ⁻¹
Thermal conductivity	32 W K ⁻¹ m ⁻¹
Melting temperature	29.78 °C
Latent heat of fusion	80,160 J kg ⁻¹
Specific heat capacity	381.5 J kg ⁻¹
Dynamic viscosity	1.81 × 10 ⁻³ kg m ⁻¹ s ⁻¹
Prandtl number	2.16 × 10 ⁻²

PCM's melting, has been carried out. The results are presented in terms of isotherms, streamlines, liquid fraction and heat transfer coefficient.

2. Description of the schematic configurations

In the present paper, numerical investigations on a cylindrical cavity filled by a solid PCM were conducted. In fact, two parametric studies were carried out on the cavity's geometry as presented in Fig. 1. We suggest considering the possibility to optimize the melting time of the PCM, through adding four thin fins on the circumference of the heated sources which are located inside the cylindrical cavity. The idea is to increase locally the heat transfer between the PCM and the external wall of the heated sources.

In the present investigation, two different cylindrical geometries filled by Gallium were studied. The geometry contains cylindrical heating sources and heating sources with fins as schematically presented in Fig. 2. The both configurations with and without thin fins were used for a fixed cylindrical surface of $S = 19,782 \text{ mm}^2$ to ensure mass conservation between the studied geometries.

The working PCM used within the heat pipe is the Gallium. The

physical properties for pure Gallium used in this investigation are given in Table 1.

A fixed temperature condition T_h is applied to the cylindrical wall. The initial temperature of the PCM is T_c as schematically presented in Fig. 1. No-slip condition is imposed at the solid surface wall, i.e., the velocity of the PCM at the wall is zero.

The objective is to study the effect of the fins integration on the melting process. Consequently, the cavity contains cylindrical heating sources and heating sources with fins as shown in Fig. 3.

The geometrical dimensions of the studied configurations are presented in Fig. 4. The both configurations contain four heating sources with and without fins to study their effect on the melting process of the PCM.

The model and the boundary conditions of the studied system are shown schematically in Fig. 5. Thanks to the symmetry of the phenomena, numerical simulations were carried out using the half of the geometry. The temperature is applied in the circumference of the cylindrical cavity while the rest is maintained adiabatic.

In order to monitor the evolution of the temperature inside the cylindrical heat pipe, the points from 1 to 13 were defined as a monitors to describe the phenomena of the melting process of the PCM as presented in Fig. 6.

A structured grids was used and the final mesh was composed of about 38,000–46,000 elements depending on which heat pipe configuration was considered as shown in Fig. 7. An optimized solution-adaptive mesh refinement is used in order to better predict the internal flow field behavior, so that a finer mesh was applied to the whole flow field for predicting correctly the features of the flow. Numerical investigations were conducted using a time step of 10^{-4} s that was found to be sufficient to give accurate results.

The main objective of the present study is to investigate numerically the heat transfer during the melting process of the PCM within two cylindrical heat pipes (see Fig. 1). This study is motivated by the need to gain improved understanding of heat transfer during the charging phase of thermal energy storage system which takes advantage of latent heat-of-fusion of PCM. A relevant consideration in such systems is the effective utilization of the heat pipe with and without fins filled by PCM by an optimum topology and disposition which is the purpose of the current paper.

3. Mathematical formulation

Unsteady two-dimensional flow models of heat transfer during the melting process of PCM inside a cylindrical cavity were governed by the general following assumptions:

- The melting of the PCM will be symmetric;
- The thermophysical properties of the PCM are constant except for the density variation with temperature, which is responsible for the generation of thermal buoyancy, for using the Boussinesq approximation;

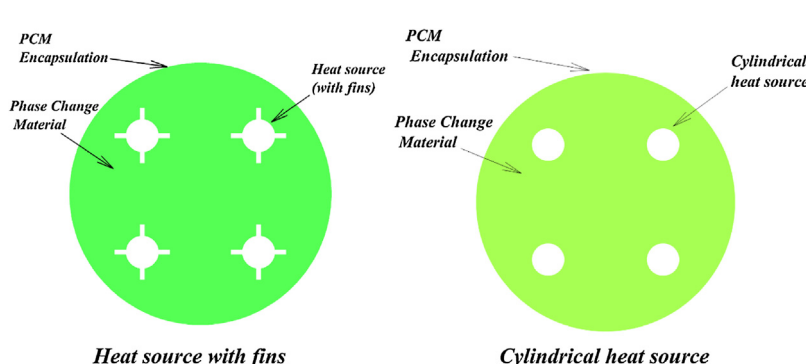


Fig. 3. Physical modeling of the cylindrical heating sources and heating sources with fins.

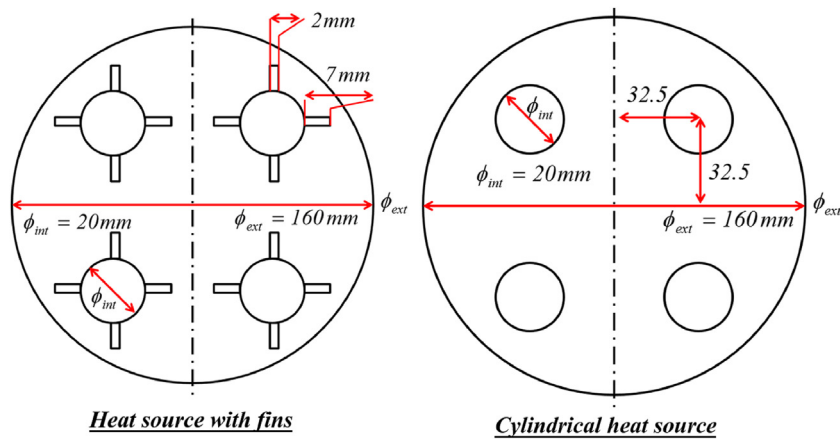


Fig. 4. Geometrical dimensions of the studied configurations.

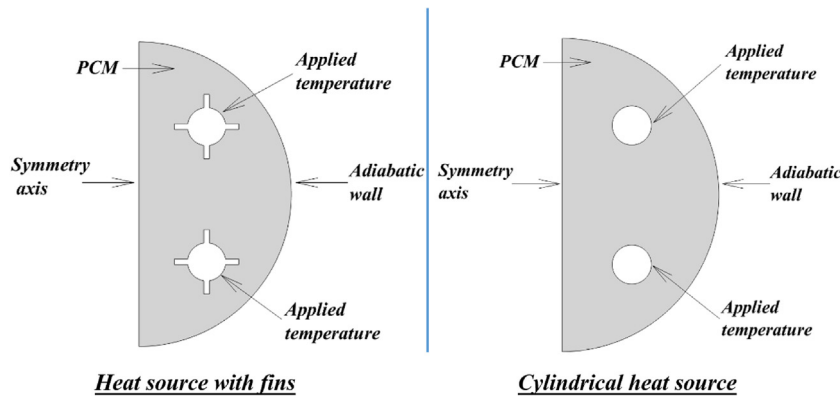


Fig. 5. Boundary conditions of the cylindrical heating sources and heating sources with fins.

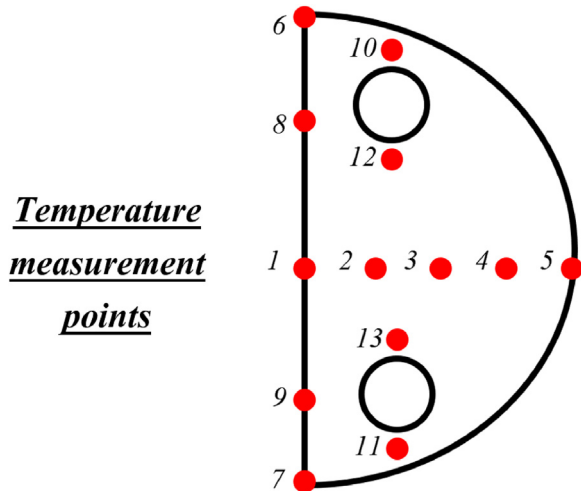


Fig. 6. Monitors of the numerical temperature measurement.

- The fluid is Newtonian and incompressible;
- The viscous dissipation is negligible;
- Fluid motion in the melt is laminar and two-dimensional.

The energy and Navier–Stokes equations were used to solve the transient hydrodynamic and thermal fields. Therefore, the resulting governing equations with consideration of gravity effect can be written as follows taking into account the foregoing assumptions.

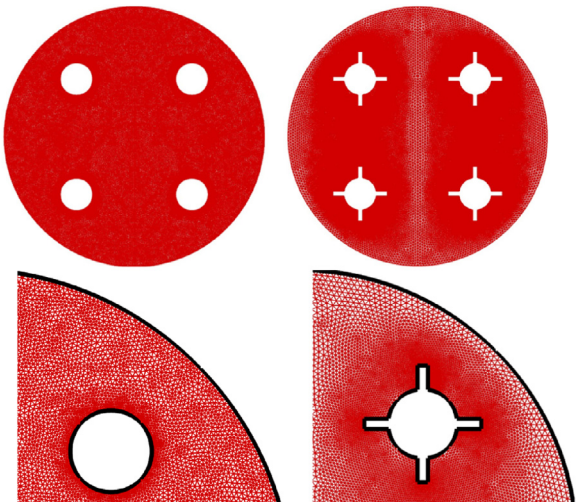


Fig. 7. Unstructured mesh grid of the configurations.

3.1. Continuity equation

The continuity equation is formulated in the following manner:

$$\frac{\partial \rho}{\partial t} + \nabla \cdot \rho \vec{u} = 0 \quad (1)$$

In Eq. (1), \vec{u} is the velocity vector and ρ is the density of the fluid.

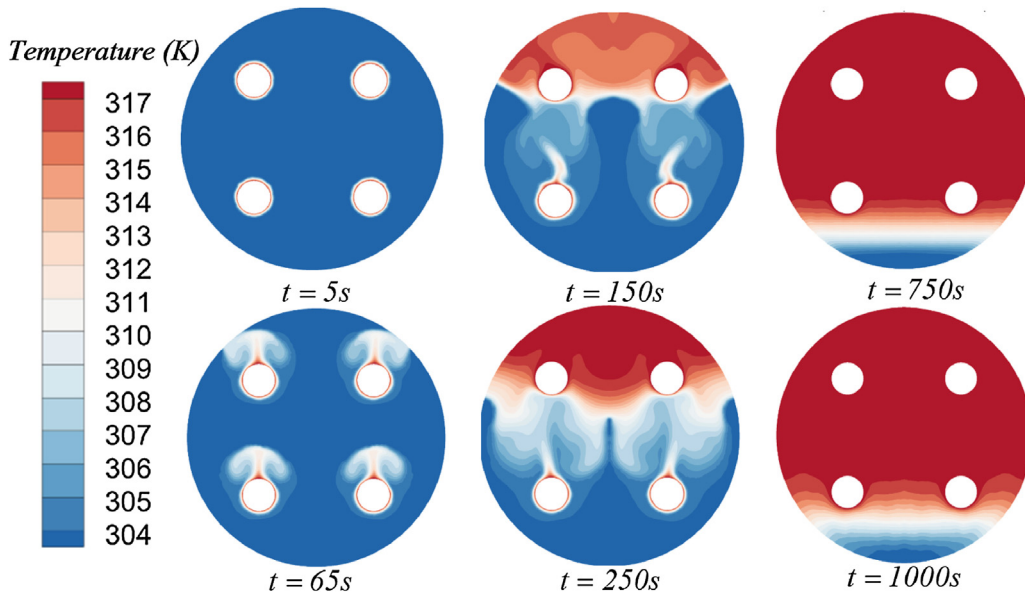


Fig. 8. Evolution of the temperature contours of the cylindrical heating sources ($T_h = 40^\circ\text{C}$).

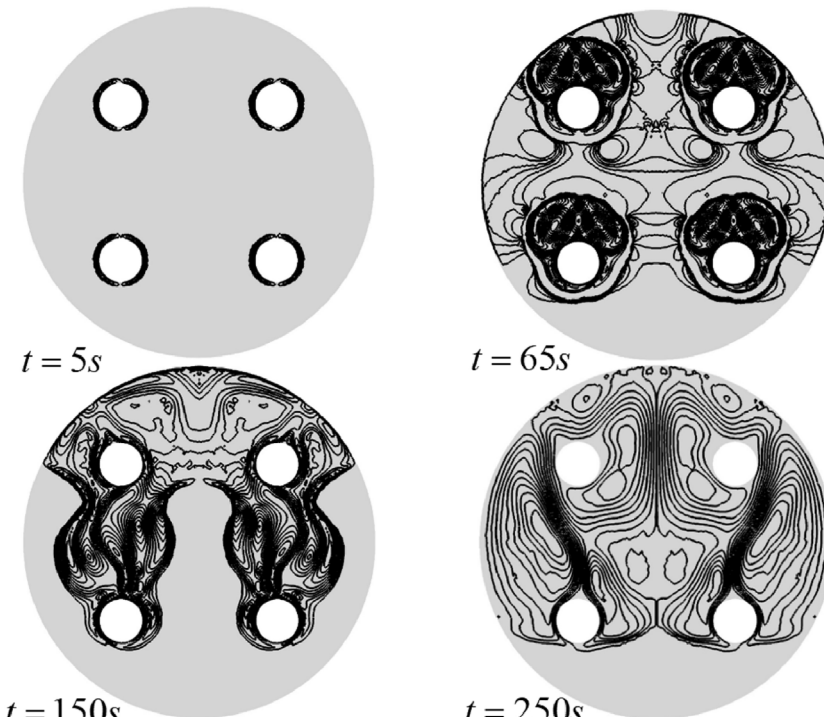


Fig. 9. Evolution of streamlines of the cylindrical heating sources ($T_h = 40^\circ\text{C}$).

3.2. Momentum equation

The following equation is the representation of the momentum equations in their vectorial forms:

$$\frac{\partial \rho \vec{u}}{\partial t} + \nabla \cdot (\rho \vec{u} \vec{u}) = -\vec{\nabla} p + \nabla \cdot \vec{\tau} + \rho \beta (T - T_m) \vec{g} \quad (2)$$

where p is the static pressure, T is the temperature, T_m is the mean temperature of the PCM, β is the coefficient of volumetric thermal expansion, \vec{g} is the acceleration of gravity vector and τ is the viscous stress tensor for a Newtonian fluid given by:

$$\vec{\tau} = \mu (\nabla u + (\nabla u)^T) \quad (3)$$

where μ is the dynamic viscosity.

3.3. Energy equation

The enthalpy of the material is computed as the sum of the sensible enthalpy, h , and the latent heat, ΔH :

$$H = h + \Delta H \quad (4)$$

where

$$h = h_{\text{ref}} + \int_{T_{\text{ref}}}^T c_p dT \quad (5)$$

where h_{ref} is the reference enthalpy, T_{ref} is the reference temperature and c_p is the specific heat at constant pressure.

The liquid fraction, α , can be defined as:

$$\begin{aligned} \alpha = 0 & \text{ if: } T < T_s, \quad \alpha = 1 & \text{ if: } T > T_l \quad \text{and} \quad \alpha = \frac{T - T_s}{T_l - T_s} \\ & \text{if: } T_s < T < T_l \end{aligned} \quad (6)$$

The latent heat content can now be written in terms of the latent heat of the material, L_F :

$$\Delta H = \alpha L_F \quad (7)$$

The latent heat content can vary between zero (for a solid) and L_F (for a liquid).

For melting problem, the energy equation is written as:

$$\frac{\partial(\rho H)}{\partial t} + \nabla \cdot (\rho \vec{u} H) = \nabla \cdot (\lambda \nabla T) + S \quad (8)$$

where λ is the thermal conductivity of the fluid, H is the enthalpy (see Eq. (4)).

The enthalpy-porosity technique treats the mushy region (partially solidified region) as a porous medium. The porosity in each cell is set equal to the liquid fraction in that cell. In fully solidified regions, the porosity is equal to zero, which extinguishes the velocities in these regions. The momentum sink S due to the reduced porosity in the mushy zone takes the following form:

$$S = \frac{(1 - \alpha)^2}{(\alpha^3 + \epsilon)} A_{\text{mush}} (\vec{u} - \vec{u}_p) \quad (9)$$

where α is the liquid volume fraction, ϵ is a small number (0.001) to prevent division by zero, A_{mush} is the mushy zone constant, and \vec{u}_p is the solid velocity due to the pulling of solidified material out of the domain (also referred to as the pull velocity).

4. Numerical procedure and mesh sensitivity study

4.1. Numerical procedure

The geometric model in Fig. 5 was created and meshed to solve the equations involving the melting and solidification process, namely the continuity, the momentum and the energy equations referring to (1), (2) and (8), respectively. An enthalpy-porosity formulation was used,

after obtaining the enthalpy field and temperature, to characterize the phase change interface.

The CFD code was accounting for two-dimensional effects. Indeed, we have modeled a 2D section passing throughout the half of the cylinder since the geometry is symmetric and all the results in term of temperature contours and streamlines were plotted on it. Working on a 2D section was adopted for decreasing the computational time and it was a suitable approach to model the PCM melting process.

Instead of following the formation of the liquid-solid front explicitly, an enthalpy-porosity formulation was used, after obtaining the enthalpy field and temperature, to characterize the phase change interface. The solution for temperature is essentially an iteration between the energy equation and the liquid fraction equation (Eq. (6)) which is directly used to update the liquid fraction usually results in poor convergence of the energy equation. The required time to simulate one configuration of the physical phenomenon under well-defined boundary conditions lasted 25 days. As a result, the parallel computing was launched on a Z600 workstation (16 CPUs, 32 GB RAM), and only half of the geometry was modeled in order to optimize the computational time.

4.2. Mesh sensitivity study

The unstructured triangular grid was used in order to provide the grid-independency of the simulation results as presented in Fig. 7. In fact, the approved grid has led to the convergence of the temperature and liquid fraction results independently of the mesh. The number of elements was increased from 38,440 and 45,834 to 44,882 and 56,668 for the cylindrical heating sources and for the heating sources with fins respectively. Moreover, great attention has been assigned to the mesh refinement of the heating sources (see Fig. 7) where a constant temperature boundary condition was applied. The aim of these meshing strategy refinements is to properly describe the physical phenomena which is developed near the heating sources.

No appreciable variation at the cylindrical cavity, for both studied configurations (cylindrical heating sources and heating sources with fins) in terms of the mean temperature value (always lower than 0.5%) was measured, ensuring the accuracy of the used meshes. Hence, it was found that the number of elements 38,440 and 45,834 for the

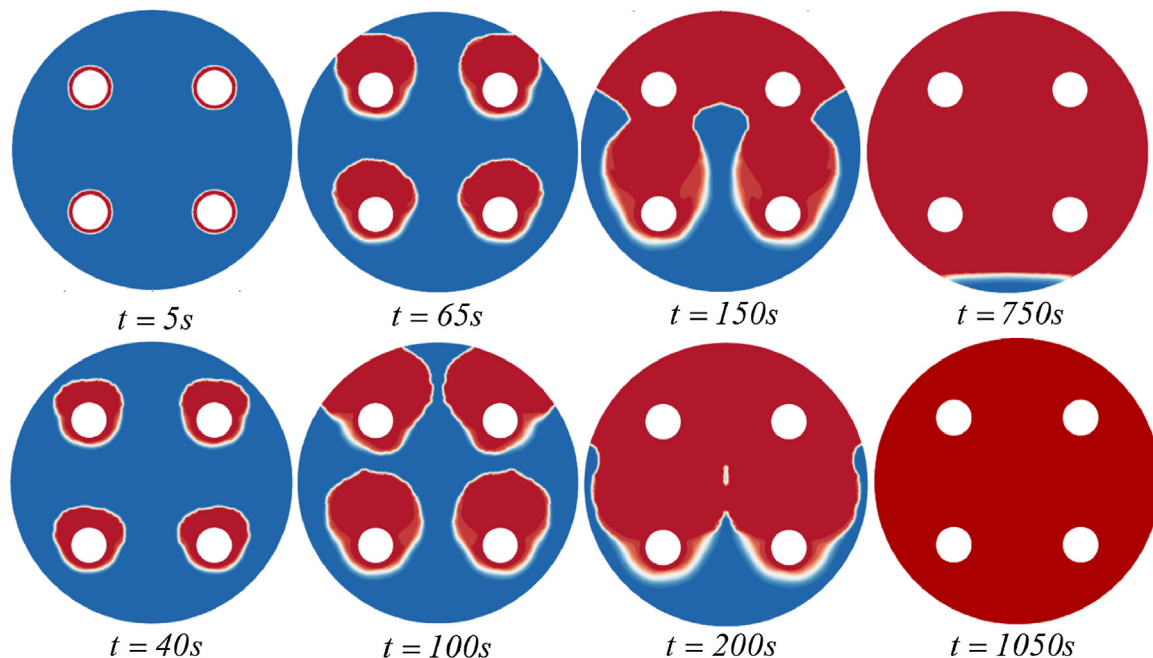


Fig. 10. Evolution of liquid fraction of cylindrical heating sources ($T_h = 40^\circ\text{C}$).

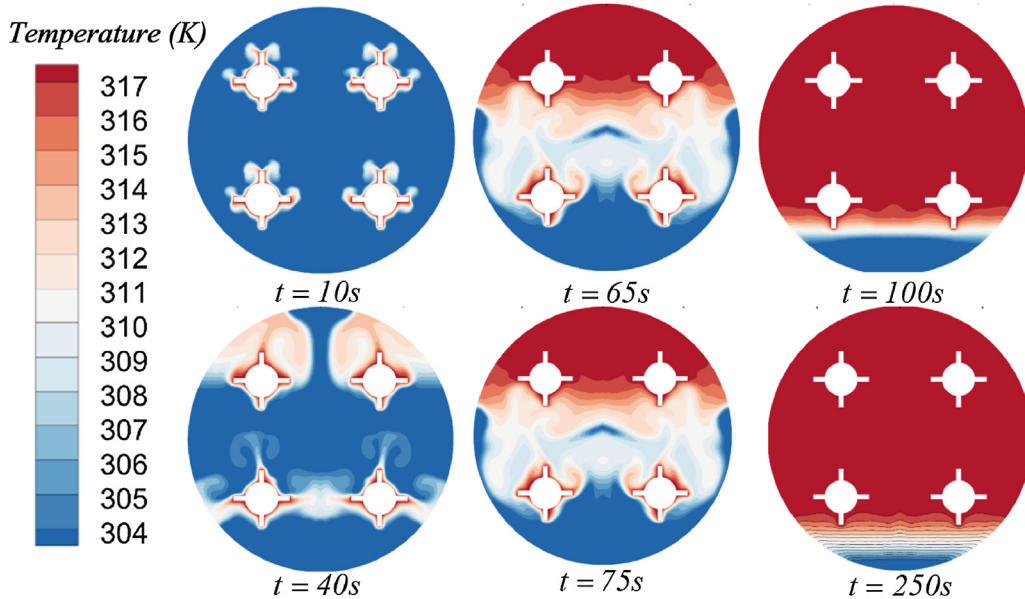


Fig. 11. Evolution of the temperature contours of heating sources with fins for $T_h = 40^\circ\text{C}$.

cylindrical heating source and the heating source with fins respectively is successfully describing the simulations ahead.

5. Results and discussion

5.1. The characteristics of the melting process for the cylindrical heating sources

The above-described physical model was used and the numerical investigations were carried out for the melting within a cylindrical cavity of a selected PCM (Gallium) which its thermophysical properties are listed in Table 1. The influence of the melting process on the temperature contours, streamlines and the liquid fraction for several times is depicted through the result illustrated in Figs. 8, 9 and 10. These plots

show the evolution of the melting process of the Gallium for the configuration without fins of the cylindrical cavity where the imposed hot temperature is $T_h = 40^\circ\text{C}$. As we can see, most of the melting occurs above and to the sides of heat sources with very little below. At early times the liquid is confined between the rigid heated cylinder and a concentric moving solid–liquid interface.

The plots (see Figs. 8–10) reveal also that at early times the melt regions are similar in shape when heat transfer within the Gallium is predominantly by conduction because the melt region is symmetrical about the axis of the cylindrical cavity. After $t = 65$ s, natural convection develops and intensifies, influencing the melt's shape in general and the melt region above the heating sources in particular. Natural convection in the melt supports the phase change process as melting continues particularly above the heating sources. However, as long as the individual melt regions have not merged to form a

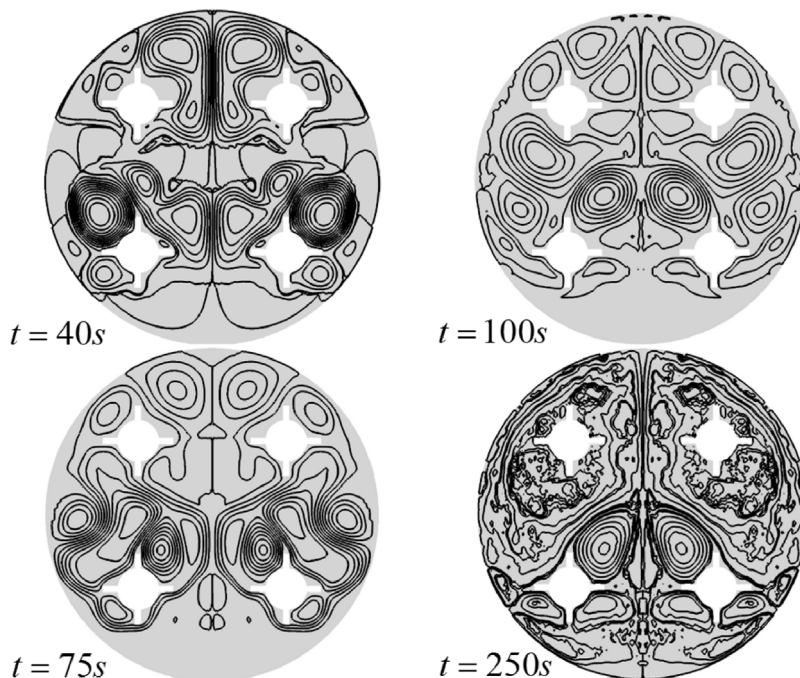


Fig. 12. Evolution of streamlines of the heating sources with fins ($T_h = 40^\circ\text{C}$).

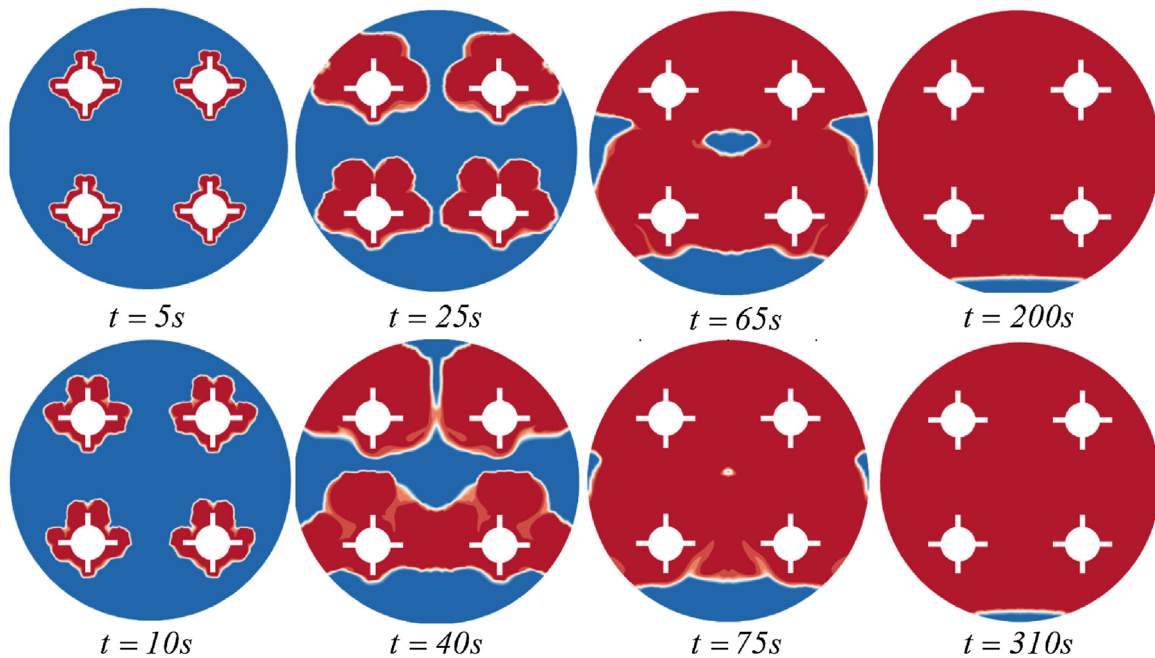


Fig. 13. Evolution of liquid fraction of heating sources with fins ($T_h = 40^\circ\text{C}$).

common liquid region around the heating sources with a common solid-liquid interface, each melt region develops independently and is not affected by the presence of other heating sources. The strong upward thrust of the melting zone is caused by natural convection. At early stages of natural convection a plume rises from the top of the heating sources at later time's circulation conveys the hot liquid to the upper part of the melt zone and in this manner continues to support the upward movement of the solid-liquid interface. As the heating continues and natural convection develops, the annular melt zone becomes increasingly distorted (see Fig. 9). As the wall temperature of the cylindrical cavity increases the solid above the heating source melts faster. Near to the liquid regions which is around the heating sources, a common boundary is formed and the natural convection surrounding the both heating sources in the bottom supports melting in the region between and above heating sources in the top.

After $t = 250$ s, the natural convection circulation in the liquid becomes more intense and influences the shape of the melt particularly in the region between and above the upper two heating sources (see Fig. 10). The plumes which rose from the top of the heating sources were unstable and affected the shape of the solid-liquid interface. When the circulation was sufficiently

intense, the plume above the both bottom heating sources was affected by the circulation between the both top heating sources and originated on the upper part of the cylindrical cavity. The plumes of the top heating sources produced nonuniform, lacerated melting shapes above the upper of the bottom heating sources.

The effect of the melting process on the temperature contours for various times for the configuration without fins is illustrated through the result depicted in Fig. 8.

The impact of the melting process on the streamlines for various times for the configuration without fins is depicted through the result illustrated in Fig. 10.

The effect of the melting process on the liquid fraction and the solid-liquid interface for several times for the configuration without fins is presented in Fig. 10. The melting time is 17.5 min.

5.2. The characteristics of the melting process for the cylindrical heating sources with fins

The effect of the melting process on the temperature contours,

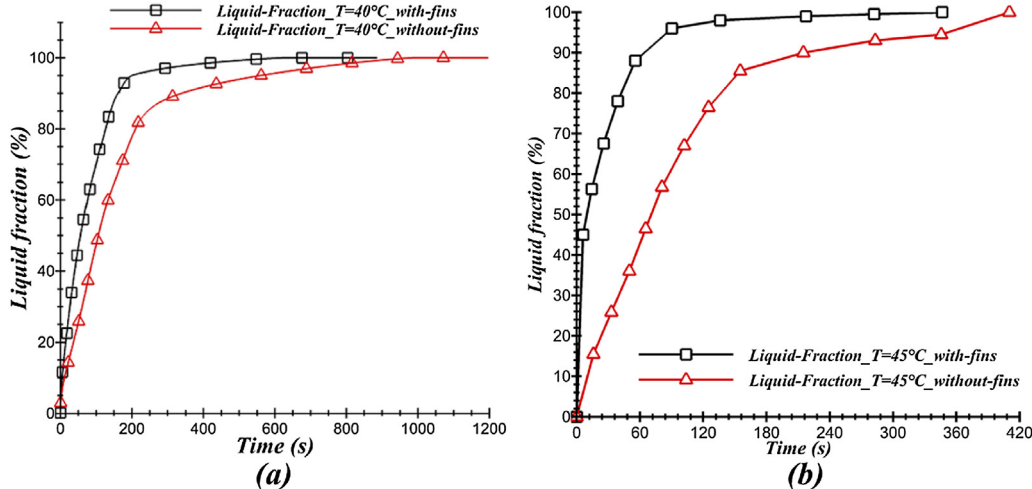


Fig. 14. Evolution of liquid fraction of the studied configurations for $T_h = 40^\circ\text{C}$ and $T_h = 45^\circ\text{C}$.

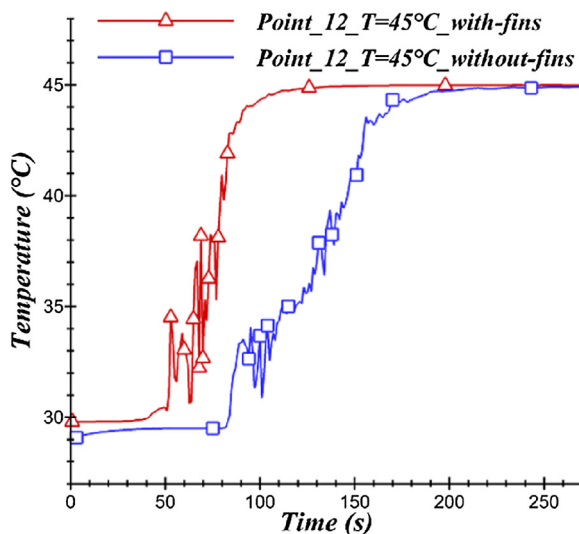


Fig. 15. Evolution of the temperature of the studied configurations at points measurement 11 and 12 for $T_h = 40^\circ\text{C}$ and $T_h = 45^\circ\text{C}$.

streamlines and the liquid fraction at different time periods is illustrated through the result depicted in Figs. 11–13. These plots show the evolution of the melting process of the Gallium for the cylindrical cavity optimized by fins where the imposed hot temperature is $T_h = 40^\circ\text{C}$. Heat transfer occurred between the hot wall of the heating sources and the solid surface of the PCM by conduction which dominated the melting process at the early stage and caused a thin layer of liquid to form in the narrow melting area because of heat transfer. During this phase state, the liquid is confined between the rigid heated source and the concentric moving solid–liquid interface. Inspection of the figures (see Figs. 11–13) reveals that at early times the melt regions are similar in shape and that when heat transfer to the Gallium is predominantly by conduction the melt region is symmetrical about the axis of the cylindrical cavity. After $t = 25$ s, natural convection develops and intensifies, influencing the melt shape in general and the melt region above the both bottom heating sources in particular. Natural convection conveys the hot liquid to the upper part of the melt zone and in this manner continues to support the upward movement of the solid–liquid interface. At $t = 75$ s, the solid–liquid interface is approximately concentric inside the cylindrical cavity (see Fig. 12). We can also observe that during the melting process the flow changes into a totally different pattern as in Fig. 13 which shows the flow transition from the base flow (single-cell) to the three cell flow at the intermediate stage and finally

to the four cell flow as time elapses. As we can observe in Fig. 12 that displays the flow behavior during the melting process for several times. After the conduction dominating stage, a complex structure of the fluid dynamics characterized by a multi-cellular flow patterns. The number and the size of the cells are dependent on the size of the molten phase. As the liquid layer increases, the number of rolls decreases. So at $t = 250$ s, when the liquid fills nearly the half of the cylindrical cavity, four counter-rotating rolls are obtained. This phenomenon is very similar to the Bénard convection due to the thermal instability. This phenomenon leads then in the sequel of calculations to the development of the above mentioned roll cells. The establishment of the vortices influences the melting kinetics of the whole cylindrical cavity.

Fig. 11 describes the evolution of the PCM temperature contours at several times for the optimized configuration by fins.

The effect of the melting process on the streamlines at various times for the optimized configuration by fins is illustrated through the result presented in Fig. 12.

The influence of the melting process on the overall liquid fraction and the solid–liquid interface versus several times for the optimized configuration by fins is depicted in Fig. 13. The melting time is 5.20 min.

5.3. Comparison between the studied configurations

The evolution of the Gallium's liquid fraction encapsulated inside the cylindrical cavity is presented in Fig. 14. Two different temperatures were applied at the heating sources $T = 40^\circ\text{C}$ (Fig. 14(a)) and $T = 45^\circ\text{C}$ (see Fig. 14(b)), knowing that the PCM melting's temperature is 29.78°C . In addition, the effect of the heating source geometry on the melting time was assessed because both of the heating sources configurations were used.

As presented in Fig. 14(a), the configuration with fins melted the PCM in 13.35 min, while the configuration without fins have melted it in 18.35 min. In this case, the melting time gained due to the integration of thin fins on the circumference of the heating source is 5 min. For Fig. 14(b) the melting time lasts 5 min with regard to the configuration with fins. For the cylindrical configuration the melting time is extended to 10 min. As a result, the melting time is estimated to be 5 min.

The temperature evolution of Gallium was monitored locally inside the cylindrical cavity as presented in Fig. 15. Thirteen points were used to gradually measure the evolution of the temperature (see Fig. 6) during the three phases that the Gallium passes through: solid phase, pasty phase and liquid phase. In Fig. 15, only the local temperature evolution for two points, namely 11 and 12 has been presented, as they highlight the contribution of the fins to the improvement of the melting time. The applied temperature in this case was $T_h = 45^\circ\text{C}$. It has been

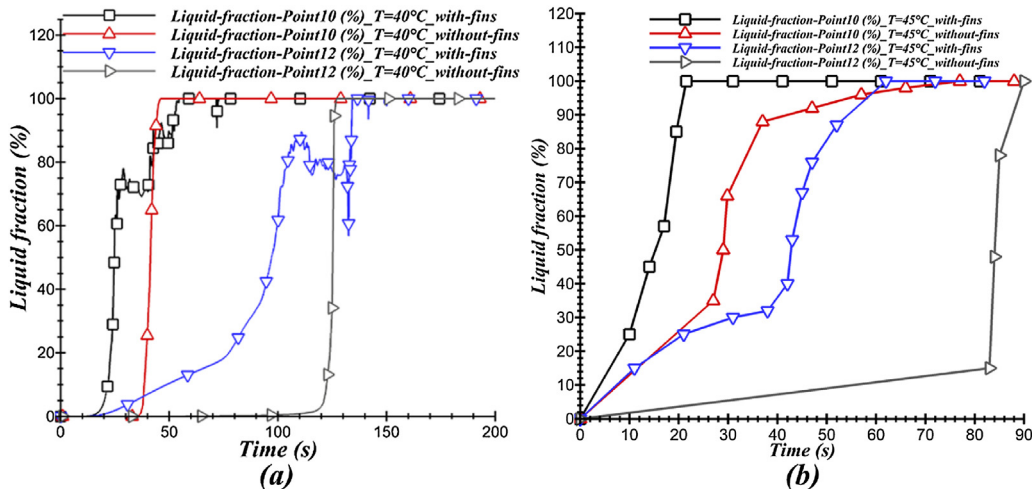


Fig. 16. Evolution of liquid fraction of the studied configurations at point measurement 10 and 12 for $T_h = 40^\circ\text{C}$ and for $T_h = 45^\circ\text{C}$.

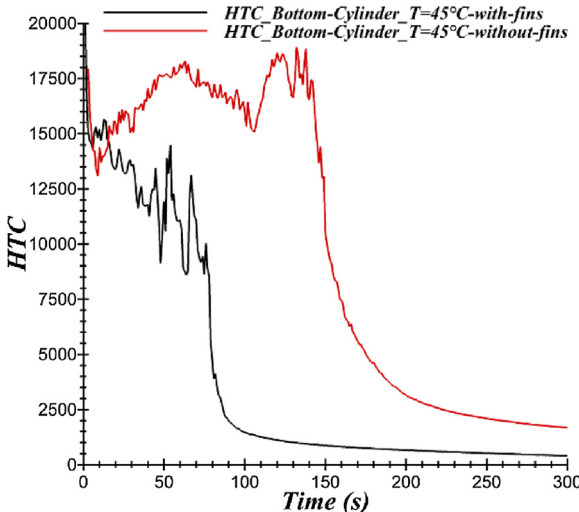


Fig. 17. Evolution of the heat transfer coefficient HTC for the studied configurations in the cylinder bottom.

found that the time required to equalize the value of the applied temperature using the heating source configuration with fins is 2 min, while it is equal to 4 min using a cylindrical heating source. The constant temperature's stage is explained by the fact that the transition to the Gallium liquid phase takes place at constant temperature.

The evolution of the local liquid fraction as a function of time for the studied configurations of the cylindrical and finned heating sources is presented in Fig. 16. The effect of two temperatures was studied $T = 40^\circ\text{C}$ (see Fig. 16(a)) and $T = 45^\circ\text{C}$ (see Fig. 16(b)). Points 10 and 12 have been defined to measure the progression of the liquid fraction within the cylindrical cavity. The fins improved the melting time. In fact, for the point 12 (Fig. 16(b)), using fins have melted the Gallium in 51 s, while the melting time for the hot cylindrical sources is 90 s. As for point 10 (Fig. 16(a)), the Gallium has melted in 40 s using the configuration with fins, while the hot cylindrical source melted it in 1 min.

5.4. Heat transfer coefficient for the studied configurations

The evolution of the heat transfer coefficient (HTC) is presented in Fig. 17. It has been monitored with regard to both configurations with and without fins for a single heating source located at the bottom of the cylinder cavity. The applied temperature in this case is $T = 45^\circ\text{C}$. The heat transfer coefficient was measured at the external wall of the

heating source. It has presented a set of fluctuations that lasted 150 s for the configuration without fins and 80 s for the configuration with fins. After these two periods of unstable variation, the heat transfer coefficient presented a decreasing rate as a function of time. The fluctuations are explained by the significant initial temperature gradient between the heating source (45°C) and the temperature of the solid Gallium's phase (29.78°C). The temperature of the melted zone in contact with the heating source increased progressively, which has led to the decrease of the measured heat transfer coefficient. As long as the configuration with fins further improves the heat transfer in the cylindrical cavity, it has been found that the curve describing the heat transfer coefficient of the fin's configuration is below the curve of the cylindrical heating source. Indeed, at $t = 300$ s, the $\text{HTC} = 2000 \text{ W/K m}^2$ for the configuration where the heating source is cylindrical, while it is equal to $\text{HTC} = 500 \text{ W/K m}^2$ for the other configuration with fins.

The evolution of the heat transfer coefficient which is measured at the top heating source of the cylindrical cavity is presented in Fig. 18. The effect of the heating source configurations with and without fins has been studied by applying two temperature values $T_h = 40^\circ\text{C}$ and $T_h = 45^\circ\text{C}$.

The curve of the heat transfer coefficient for the configuration with fins remains under the curve of the hot cylindrical source configuration. Therefore, it is concluded that the fins added at the hot source enhance the heat transfer and improve the melting time of the Gallium.

6. Conclusion

The melting process along a cylindrical cavity filled with a PCM (Gallium), where four heating sources were included, has been performed through this paper using two-dimensional CFD simulations. The physical enthalpy-porosity formulation of the CFD model has been used. The aim of this work essentially focuses on the thermal energy storage improvement by using an innovative geometrical form which accelerates the melting time of the Gallium and optimizes the efficiency of the heating sources according to the applied temperatures. In fact, two configurations were assessed, the first configuration with a cylindrical heating sources, and the second configuration with four thin fins distributed over the circumference of the heating sources. The parametric studies were carried out using the validated models and the main conclusions drawn from these numerical studies are presented as follows:

- Integrating fins at each heating source have enhanced the heat transfer in the PCM located inside the cylindrical cavity and improved its melting time from 18.35 min to 13.35 min while applying a hot temperature ($T_h = 40^\circ\text{C}$).

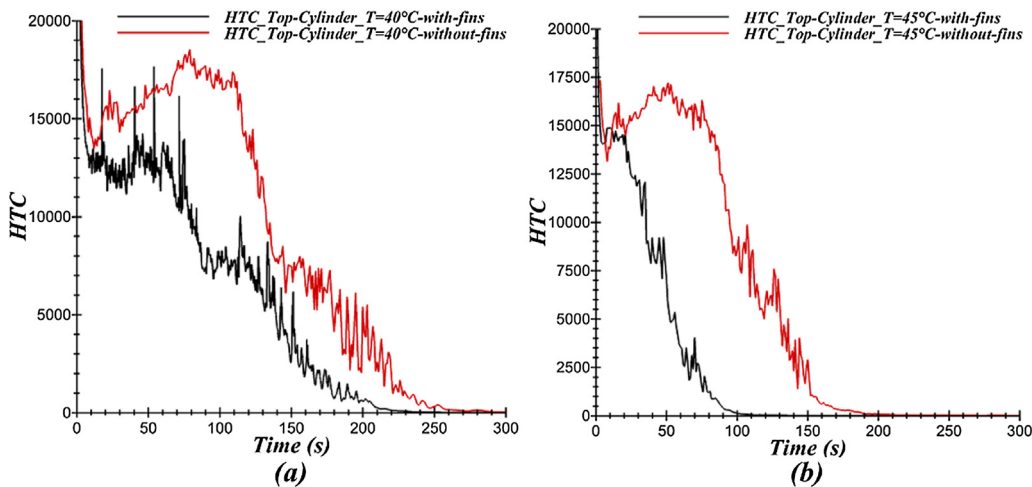


Fig. 18. Evolution of the heat transfer coefficient HTC for the studied configurations in the cylinder top for $T_h = 40^\circ\text{C}$ and $T_h = 45^\circ\text{C}$.

- The evolution of the temperature, liquid fraction and streamlines contours for the studied configurations which correspond to the cylindrical heating sources and the heating sources with fins for two applied temperatures ($T_h = 40^\circ\text{C}$) and ($T_h = 45^\circ\text{C}$) were investigated to explain the effect of the geometric design in the melting time.
- Temperature and liquid fraction measurement were assessed numerically for some specific points located inside the studied configurations in order to determine the redesign effect of the heating sources.
- The heat transfer coefficient at the heating sources has been defined as indicator of performance to measure the contribution of the fins in the improvement of the melting time within the cylindrical cavity. It is concluded that the fins added at the hot source enhance the heat transfer and improve the melting time of Gallium.

References

- S. Mat, A.A. Al-Abidi, K. Sopian, M.Y. Sulaiman, A.T. Mohammad, Enhance heat transfer for PCM melting in triplex tube with internal–external fins, *Energy Convers. Manag.* 74 (2013) 223–236.
- R.M. Saeed, J. Schlegel, C. Castano, R. Sawafta, Preparation and enhanced thermal performance of novel (solid to gel) form-stable eutectic PCM modified by nanographene platelets, *J. Energy Storage* 15 (2018) 91–102, <http://dx.doi.org/10.1016/j.est.2017.11.003> <http://www.sciencedirect.com/science/article/pii/S2352152X17304127>.
- S. Álvarez, L.F. Cabeza, A. Ruiz-Pardo, A. Castell, J.A. Tenorio, Building integration of PCM for natural cooling of buildings, *Appl. Energy* 109 (2013) 514–522.
- G. Diarce, Á. Campos-Celador, K. Martín, A. Urresti, A. García-Romero, J. Sala, A comparative study of the CFD modeling of a ventilated active façade including phase change materials, *Appl. Energy* 126 (2014) 307–317.
- N. Tay, F. Bruno, M. Belusko, Experimental validation of a CFD model for tubes in a phase change thermal energy storage system, *Int. J. Heat Mass Transfer* 55 (4) (2012) 574–585.
- H. Sattari, A. Mohebbi, M. Afsahi, A.A. Yancheshme, CFD simulation of melting process of phase change materials (PCMs) in a spherical capsule, *Int. J. Refrig.* 73 (2017) 209–218, <http://dx.doi.org/10.1016/j.ijrefrig.2016.09.007> <http://www.sciencedirect.com/science/article/pii/S0140700716302870>.
- F. Liu, J. Wang, X. Qian, Integrating phase change materials into concrete through microencapsulation using cenospheres, *Cement Concr. Compos.* 80 (2017) 317–325, <http://dx.doi.org/10.1016/j.cemconcomp.2017.04.001> <http://www.sciencedirect.com/science/article/pii/S0958946516303432>.
- K. Kumarasamy, J. An, J. Yang, E.-H. Yang, Novel CFD-based numerical schemes for conduction dominant encapsulated phase change materials (EPCM) with temperature hysteresis for thermal energy storage applications, *Energy* 132 (2017) 31–40, <http://dx.doi.org/10.1016/j.energy.2017.05.054> <http://www.sciencedirect.com/science/article/pii/S0360544217307612>.
- K. Kant, A. Shukla, A. Sharma, Heat transfer studies of building brick containing phase change materials, *Solar Energy* 155 (2017) 1233–1242, <http://dx.doi.org/10.1016/j.solener.2017.07.072> <http://www.sciencedirect.com/science/article/pii/S0038092X17306576>.
- M. Saffari, A. de Gracia, S. Ushak, L.F. Cabeza, Passive cooling of buildings with phase change materials using whole-building energy simulation tools: a review, *Renew. Sustain. Energy Rev.* 80 (2017) 1239–1255, <http://dx.doi.org/10.1016/j.rser.2017.05.139> <http://www.sciencedirect.com/science/article/pii/S136403211730758X>.
- C. Wang, T. Lin, N. Li, H. Zheng, Heat transfer enhancement of phase change composite material: copper foam/paraffin, *Renew. Energy* 96 (2016) 960–965, <http://dx.doi.org/10.1016/j.renene.2016.04.039> <http://www.sciencedirect.com/science/article/pii/S096014811630341X>.
- F. Kuznik, K. Johannes, E. Franquet, L. Zalewski, S. Gibout, P. Tittlein, J.-P. Dumas, D. David, J.-P. Bédécarrats, S. Lassue, Impact of the enthalpy function on the simulation of a building with phase change material wall, *Energy Build.* 126 (2016) 220–229, <http://dx.doi.org/10.1016/j.enbuild.2016.05.046> <http://www.sciencedirect.com/science/article/pii/S0378778816304157>.
- S. Park, S. Woo, J. Shon, K. Lee, Numerical model and simulation of a vehicular heat storage system with phase-change material, *Appl. Therm. Eng.* 113 (2017) 1496–1504, <http://dx.doi.org/10.1016/j.applthermaleng.2016.11.162> <http://www.sciencedirect.com/science/article/pii/S1359431116335669>.
- T. Zhou, X. Liu, Y. Li, Z. Sun, J. Zhou, Dynamic measurement of the thermal conductivity of phase change materials in the liquid phase near the melting point, *Int. J. Heat Mass Transfer* 111 (2017) 631–641, <http://dx.doi.org/10.1016/j.ijheatmasstransfer.2017.04.020> <http://www.sciencedirect.com/science/article/pii/S0038092X17301939>.
- M.C. Browne, E. Boyd, S.J. McCormack, Investigation of the corrosive properties of phase change materials in contact with metals and plastic, *Renew. Energy* 108 (2017) 555–568, <http://dx.doi.org/10.1016/j.renene.2017.02.082> <http://www.sciencedirect.com/science/article/pii/S096014811730174X>.
- M. Chaabane, H. Mhiri, P. Bournot, Thermal performance of an integrated collector storage solar water heater (ICSSWH) with phase change materials (PCM), *Energy Convers. Manag.* 78 (2014) 897–903.
- F. Kaplan, C. De Vivero, S. Howes, M. Arora, H. Homayoun, W. Burleson, D. Tullsen, A.K. Coskun, Modeling and analysis of phase change materials for efficient thermal management, 2014 32nd IEEE International Conference on Computer Design (ICCD), IEEE, 2014, pp. 256–263.
- T. Ma, H. Yang, Y. Zhang, L. Lu, X. Wang, Using phase change materials in photovoltaic systems for thermal regulation and electrical efficiency improvement: a review and outlook, *Renew. Sustain. Energy Rev.* 43 (2015) 1273–1284.
- M. Muhammad, O. Badr, H. Yeung, Validation of a CFD melting and solidification model for phase change in vertical cylinders, *Numer. Heat Transfer Part A: Appl.* 68 (5) (2015) 501–511.
- R. Sharma, P. Ganesan, J. Sahu, H. Metselaar, T. Mahlia, Numerical study for enhancement of solidification of phase change materials using trapezoidal cavity, *Powder Technol.* 268 (2014) 38–47, <http://dx.doi.org/10.1016/j.powtec.2014.08.009> <http://www.sciencedirect.com/science/article/pii/S0032591014007098>.
- K. Pieliuchowska, K. Pieliuchowski, Phase change materials for thermal energy storage, *Prog. Mater. Sci.* 65 (2014) 67–123.
- M. Temirel, H. Hu, H. Shabgard, P. Boettcher, M. McCarthy, Y. Sun, Solidification of additive-enhanced phase change materials in spherical enclosures with convective cooling, *Appl. Therm. Eng.* 111 (2017) 134–142, <http://dx.doi.org/10.1016/j.applthermaleng.2016.09.090> <http://www.sciencedirect.com/science/article/pii/S1359431116317057>.
- D. Cano, C. Funéz, L. Rodriguez, J. Valverde, L. Sanchez-Silva, Experimental investigation of a thermal storage system using phase change materials, *Appl. Therm. Eng.* 107 (2016) 264–270, <http://dx.doi.org/10.1016/j.applthermaleng.2016.06.169> <http://www.sciencedirect.com/science/article/pii/S1359431116310833>.
- L. Zhao, Y. Xing, Z. Wang, X. Liu, The passive thermal management system for electronic device using low-melting-point alloy as phase change material, *Appl. Therm. Eng.* 125 (2017) 317–327, <http://dx.doi.org/10.1016/j.applthermaleng.2017.07.004> <http://www.sciencedirect.com/science/article/pii/S1359431117309973>.
- V. Kapsalis, D. Karamanis, Solar thermal energy storage and heat pumps with phase change materials, *Appl. Therm. Eng.* 99 (2016) 1212–1224, <http://dx.doi.org/10.1016/j.applthermaleng.2016.01.071> <http://www.sciencedirect.com/science/article/pii/S1359431116300217>.
- W. Zhao, S. Neti, A. Oztekin, Heat transfer analysis of encapsulated phase change materials, *Appl. Therm. Eng.* 50 (1) (2013) 143–151, <http://dx.doi.org/10.1016/j.applthermaleng.2012.06.016> <http://www.sciencedirect.com/science/article/pii/S135943112004371>.
- S. ed Dén Fertahi, T. Bouhal, A. Arid, T. Kousksou, A. Jamil, N. Moujibi, A. Benbassou, Thermo-mechanical strength analysis for energy storage improvement of horizontal storage tanks integrating evacuated tube collectors, *Int. J. Hydrogen Energy* 42 (49) (2017) 29370–29383, <http://dx.doi.org/10.1016/j.ijhydene.2017.10.016> <http://www.sciencedirect.com/science/article/pii/S0360319917339137>.
- S. ed Dén Fertahi, T. Bouhal, Y. Agrouaz, T. Kousksou, T.E. Rhafiki, Y. Zeraouli, Performance optimization of a two-phase closed thermosyphon through CFD numerical simulations, *Appl. Therm. Eng.* 128 (2018) 551–563, <http://dx.doi.org/10.1016/j.applthermaleng.2017.09.049> <http://www.sciencedirect.com/science/article/pii/S1359431117339558>.
- T. Bouhal, S. Fertahi, Y. Agrouaz, T.E. Rhafiki, T. Kousksou, A. Jamil, Numerical modeling and optimization of thermal stratification in solar hot water storage tanks for domestic applications: CFD study, *Solar Energy* 157 (2017) 441–455, <http://dx.doi.org/10.1016/j.solener.2017.08.061> <http://www.sciencedirect.com/science/article/pii/S0038092X17307429>.
- T. Bouhal, S. ed Dén Fertahi, Y. Agrouaz, T.E. Rhafiki, Y. Zeraouli, A. Jamil, Towards an energy efficiency optimization of solar horizontal storage tanks and circulation pipes integrating evacuated tube collectors through CFD parametric studies, *Sustain. Energy Technol. Assess.* 26 (2018) 93–104, <http://dx.doi.org/10.1016/j.seta.2017.10.004> <http://www.sciencedirect.com/science/article/pii/S2213138817303909>.
- T. Bouhal, Y. Agrouaz, A. Allouhi, T. Kousksou, A. Jamil, T.E. Rhafiki, Y. Zeraouli, Impact of load profile and collector technology on the fractional savings of solar domestic water heaters under various climatic conditions, *Int. J. Hydrogen Energy* 42 (18) (2017) 13245–13258, <http://dx.doi.org/10.1016/j.ijhydene.2017.03.226> <http://www.sciencedirect.com/science/article/pii/S0360319917312776>.
- S. ed Dén Fertahi, T. Bouhal, F. Gargab, A. Jamil, T. Kousksou, A. Benbassou, Design and thermal performance optimization of a forced collective solar hot water production system in morocco for energy saving in residential buildings, *Solar Energy* 160 (2018) 260–274, <http://dx.doi.org/10.1016/j.solener.2017.12.015> <http://www.sciencedirect.com/science/article/pii/S0038092X17310873>.